INSTITUTES FOR ENVIRONMENTAL RESEARCH
National Severe Storms Laboratory
Norman, Oklahoma

April, 1967

Thunderstorm Circulations and Turbulence Studies from Aircraft and Radar Data

JAMES C. FANKHAUSER

J. T. LEE

Technical Memorandum IERTM-NSSL 32

U.S. DEPARTMENT OF COMMERCE / ENVIRONMENTAL SCIENCE SERVICES ADMINISTRATION

ENVIRONMENTAL SCIENCE SERVICES ADMINISTRATION

INSTITUTES FOR ENVIRONMENTAL RESEARCH

NATIONAL SEVERE STORMS LABORATORY TECHNICAL MEMORANDA

The National Severe Storms Laboratory, Norman, Oklahoma, in cooperation with other government groups, and with units of commerce and education, seeks to increase understanding of severe local storms, to improve methods for detecting these storms and for measuring associated meteorological parameters, and to promote the development and applications of weather radar.

Reports by the cooperating groups are printed as NSSL Technical Memoranda, a sub-series of the ESSA Technical Memorandum series, to facilitate prompt communication of information to vitally interested parties and to elicit their constructive comments. These Memoranda are not formal scientific publications.

The NSSL Technical Memoranda, beginning with No. 28, continue the sequence established by the U.S. Weather Bureau National Severe Storms Project, Kansas City, Missouri. Numbers 1-22 were designated NSSP Reports. Numbers 23-27 were NSSL Reports, and 24-27 appeared as a subseries of Weather Bureau Technical Notes.

Reports in this series are available from the Clearinghouse for Federal Scientific and Technical Information, U.S.Department of Commerce, Sills Bldg., Port Royal Road, Springfield, Virginia 22151.

U.S. DEPARTMENT OF COMMERCE
ENVIRONMENTAL SCIENCE SERVICES ADMINISTRATION
INSTITUTES FOR ENVIRONMENTAL RESEARCH

Institutes for Environmental Research Technical Memorandum - NSSL-32

SOME PHYSICAL AND DYNAMICAL ASPECTS OF A SEVERE RIGHT MOVING CUMULONIMBUS

James C. Fankhauser

ASSOCIATION BETWEEN ATMOSPHERIC TURBULENCE AND RADAR ECHOES IN OKLAHOMA

J. T. Lee

U.S. NATIONAL SEVERE STORMS LABORATORY
TECHNICAL MEMORANDUM NO. 32

NORMAN, OKLAHOMA
March 1967

FOREWORD

The studies presented here have been made possible through the cooperation and substantial support of the Aeronautical Systems Division, U. S. Air Force; the Federal Aviation Agency; the U. S. Navy; and the Research Flight Facility, Institute for Atmospheric Sciences, ESSA.

TABLE OF CONTENTS

		Page
ASSOCIATION BETWEEN ATMOSPHERIC TURBULENCE AND RADAR ECHOES IN OKLAHOMA J. T. Lee		1
	Abstract	1
1	Introduction	1
2	Data Acquisition	2
3	Data Analysis	3
4	Summary	8
	References	9
SOME PHYSICAL AND DYNAMICAL ASPECTS OF A SEVERE RIGHT MOVING CUMULONIMBUS J. C. Fankhauser		11
	Abstract	11
1	Introduction	11
2	Synoptic Situation, Cloud Features, and Storm Morphology	11
3	Kinematic Properties of the Near-Cloud Environment	16
4	Storm Motion in Response to Possible Steering Forces	22
5	Moisture and Energy Budget Considerations	25
6	Summary	30
	Acknowledgements	31
	References	31

ASSOCIATION BETWEEN ATMOSPHERIC TURBULENCE AND RADAR ECHOES IN OKLAHOMA

J. T. Lee
National Severe Storms Laboratory

ABSTRACT

Turbulence experienced by aircraft during penetration of Oklahoma thunderstorms is compared with the characteristics of associated radar echoes. The correlation coefficient between the standard deviation of the derived gust velocity and the maximum radar reflectivity of the penetrated storm is about .55, according to data collected during 87 storm flights made by a USAF F-100 aircraft during 1964 and 1965. The correlation between the standard deviation and radar reflectivity gradient is less than 0.3. Other characteristics of the radar echo such as maximum reflectivity gradient, maximum reflectivity along flight path, and average gradient of reflectivity along the flight path are investigated, but are not found to contribute appreciably to the estimation of turbulence. At present, the maximum radar reflectivity of a storm seems to be the best indicator of turbulence encountered by an aircraft. The data show a lower frequency of severe turbulence at 37,000 feet altitude than at 27,000 feet, though the incidence of weaker categories is about the same.

1. INTRODUCTION

The Federal Aviation Agency, National Aeronautics and Space Administration, British Royal Aircraft Establishment, Air Force Aeronautical Systems Division (ASD), U.S. Navy, and National Severe Storms Laboratory (NSSL) have pooled personnel, aircraft, and funds to study turbulence in and near convective clouds. This report is based on data obtained from 87 penetrations made by ASD F-100F aircraft in 1964 and 1965 and 40 penetrations by an F-11 aircraft in 1964.

An objective of the program is to associate radar echo characteristics with turbulence in and near convective clouds. The main guide lines in the penetration program have been stated before [1] but are reiterated as follows:

1. Sampling was confined to one flight level.

2. Thunderstorms were within optimum radar range; i.e., 20 to 100 n.mi. radius of Norman.

3. Reflectivity factors (Z_e) in the storm were not to exceed $10^5 mm^6/m^3$.

4. Thunderstorms satisfying (2) and (3) above were sampled on a random basis.

2. DATA ACQUISITION

The radar observations were coordinated in time and space with aircraft flight paths, by referencing aircraft and radar operations to the same master clock. The primary radar was the WSR-57 located in Norman, Oklahoma, equipped with both a step-attenuation program and a contoured echo intensity presentation (Figure 1) [2]. Radar data processing has been discussed by Gray and Wilk [3]. The radar reflectivity (Z_e) used in this paper has been discussed by Battan [4] and by Wilk and Kulshrestha [5].

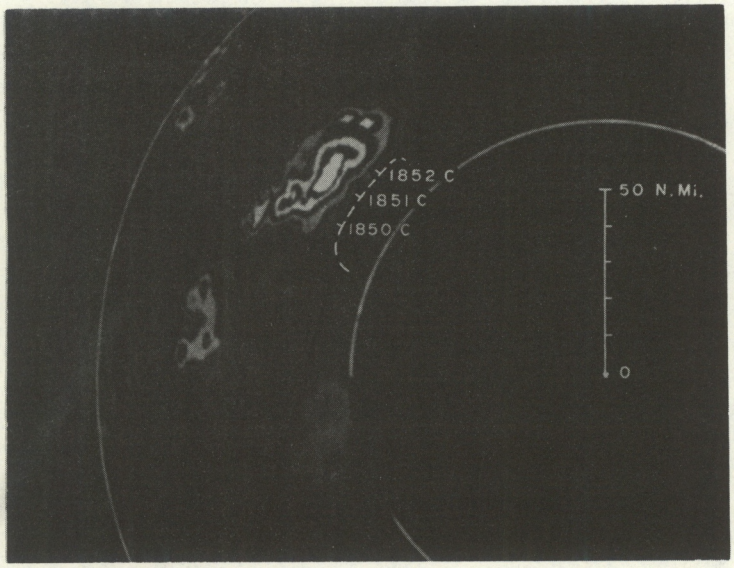

2451 UT

Fig. 1 - Integrated log-contour radar scope display at 1851 C, May 25, 1965. Corresponding aircraft track is superimposed and is shown as a dashed line.

F-100 instrumentation included gust vanes, accelerometers, rate gyros, free air temperature sensor (Rosemount type), pressure, and other sensing equipment described by Miller [6]. The F-11 data was obtained with a VGH (Velocity-Gust-Height) recorder and a photographed instrument panel. In 1965, F-100 rudder and elevator positions were also recorded, to help evaluate the gust measuring equipment and determine pilot inputs which tend to mask the turbulence data. Derived gust velocities (U_{de}) were computed following the method of Pratt [7]. Maximum values and standard deviations of U_{de} were used as turbulence indicators. Aircraft data were correlated with various radar echo characteristics as detailed in a previous paper [1].

Flight operations were conducted during April, May and early June with the greatest activity occurring during the month of May.

3. DATA ANALYSIS

Flight data were obtained primarily near 27,000-ft. pressure altitude in 1964. In 1965 the principal sampling altitude was 37,000 ft., not far below the ceiling of commercial jet operations. In 1964 nearly all flights passed through storm centers, while the 1965 flights were designed to pass through the edges of large storms -- sometimes missing the centers by as much as 15 n. mi.

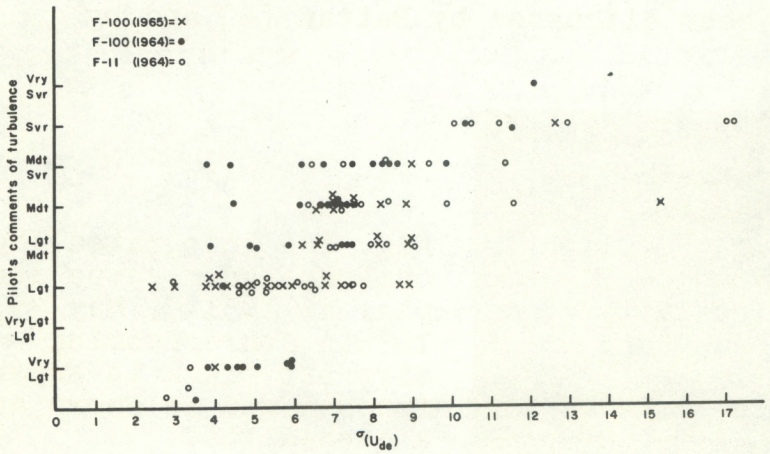

Fig. 2 - Pilots' evaluation of turbulence compared to computed standard deviation of derived gust velocities.

Figure 2 compares the pilots' characterization of turbulence during particular flights with corresponding standard deviations of derived gust velocities $\sigma(U_{de})$. Although the pilot and instrument evaluations generally agree, only $(U_{de})_{max}$ and $\sigma(U_{de})$ are used in the radar echo-turbulence comparison. Table 1 relates values of U_{de} and $\sigma(U_{de})$ to various turbulence categories.

Table 1. Turbulence Categories

Turbulence Category	U_{de} Values (fps)	$\sigma(U_{de})$ (fps)
Light	Less than 20	0 - 6
Moderate	20 - 34	6 - 8
Severe	35 - 50	8 - 15
Extreme	Above 50	Above 15

Because Lappe's analysis [8] of 1965 test flights shows that a 0.5 degree change in elevator position can produce a 0.1 g change in the recorded acceleration, all portions of the 1965 flights exhibiting large pilot input (0.5 degree elevator movement) were removed from the data sample. Radar data used are similar to the digitized format discussed by Kessler and Russo [9]; and all analyses are based on square grid spacings of 2.5 n. mi.

Figure 3 compares $\sigma(U_{de})$ and the maximum radar echo intensity (maximum storm reflectivity factor, Z_e) of cells recorded during aircraft penetrations. Figure 4 shows $(U_{de})_{max}$ for each penetration with the corresponding $(Z_e)_{max}$ of the cell under observation. The similarity between the two graphs is supported by consideration of Figure 5, which shows a linear relationship between $(U_{de})_{max}$ and $\sigma(U_{de})$ during 1965. (The correlation coefficient $r = 0.89$.)

Since the standard deviation is not greatly influenced by extremes, the correlation coefficients involving $\sigma(U_{de})$ are higher than those with $(U_{de})_{max}$.

The distributions of $\sigma(U_{de})$ against

(a) $Z_{e(max)}$ along the flight path,

(b) maximum reflectivity gradient ($dZ_e/dx\ _{max}$) along the flight path, and

(c) average reflectivity gradient $\overline{(dZ_e/dx)}$ along the flight path

are shown in Figures 6, 7, and 8, respectively. Table 2 lists corresponding correlation coefficients for 1964 and 1965 data.

The storms investigated in 1964 and 1965 were approximately the same size, and it seems that the lower correlation coefficient between turbulence and reflectivity gradient in 1965 may be related to the larger percentage of 1965 flights conducted far from the core of maximum radar reflectivity. Probably the higher 1964 correlation reflects principally the tendency for $Z_{e(max)}$ and its gradient to be more positively correlated when the latter is calculated along a path through the storm core.

Combinations of maximum reflectivity gradient to indicate turbulence have been discussed previously [1], and data obtained in 1965 (Table 2) reinforce earlier indications that the parameters in combination are little better than the reflectivity taken alone.

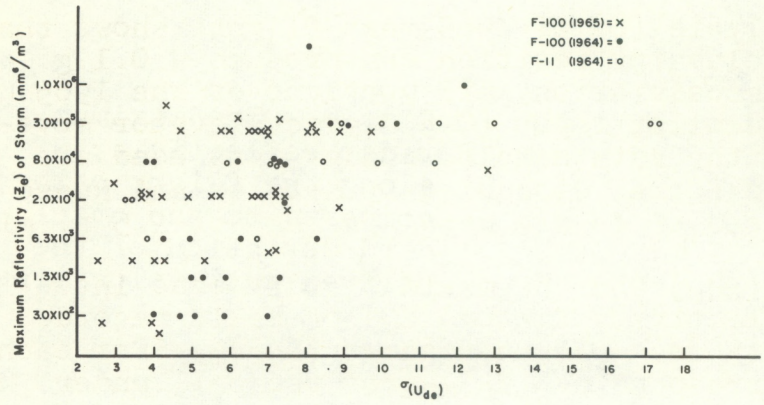

Fig. 3 - Standard deviation of derived gust velocities of each penetration compared to the maximum radar reflectivity.

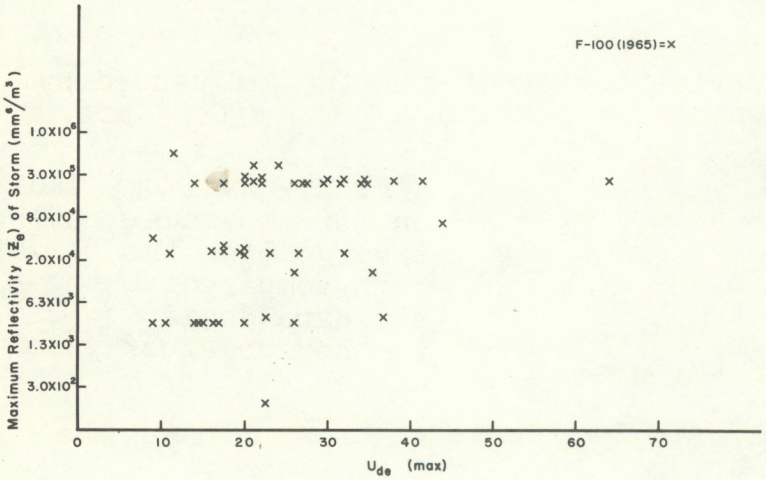

Fig. 4 - Maximum derived gust velocity related to maximum radar reflectivity.

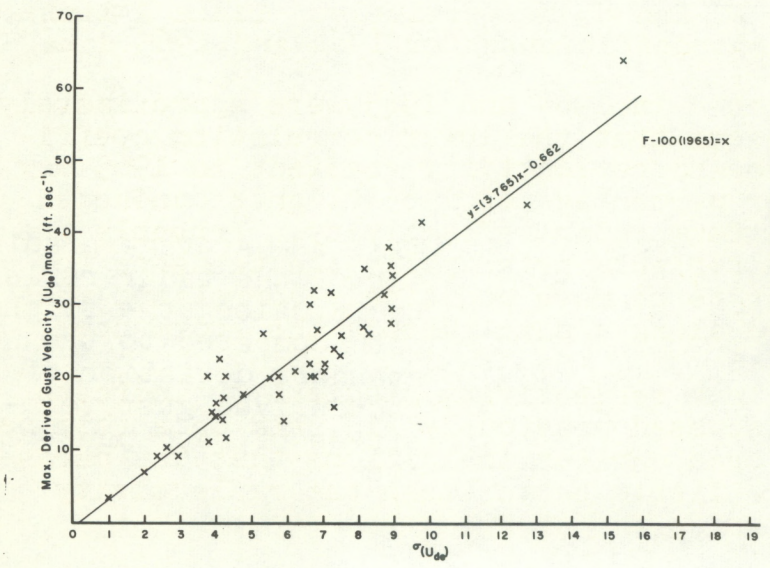

Fig. 5 - Comparison of the 1965 standard deviation of the derived gust velocities and the maximum derived gust velocities for each penetration.

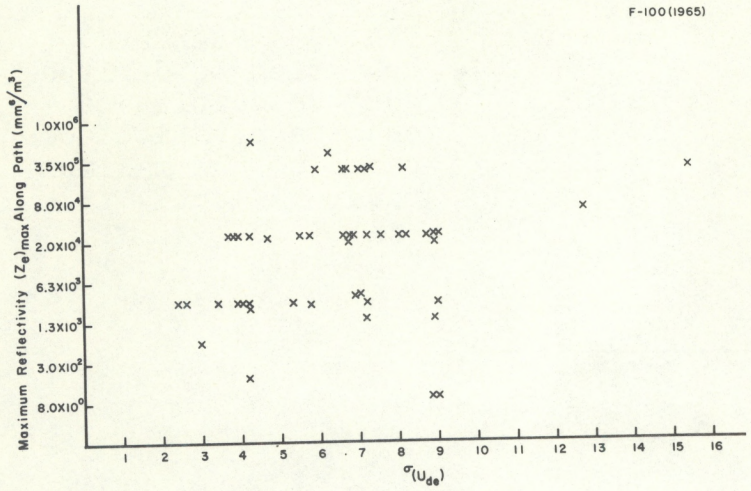

Fig. 6 - The maximum radar reflectivity along the flight path compared to the standard deviation of the derived gust velocities.

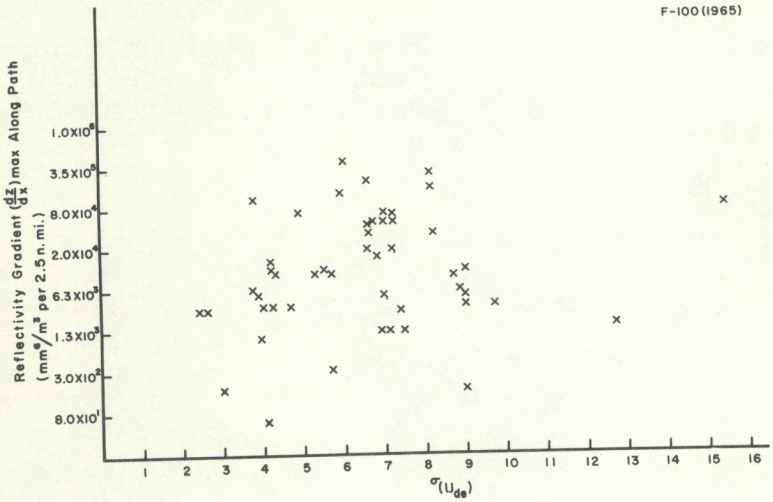

Fig. 7 - Maximum gradient of the radar reflectivity along the flight path compared to the standard deviation of the derived gust velocities.

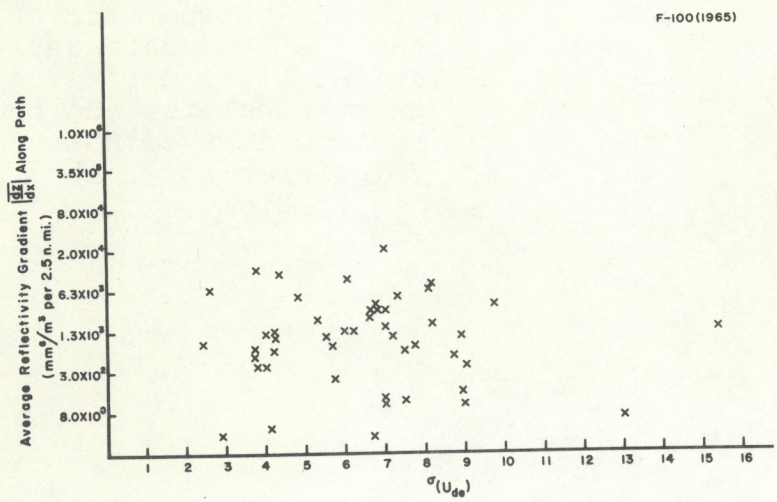

Fig. 8 - Average gradient of the radar reflectivity along the flight path compared to the standard deviation of the derived gust velocities of each penetration.

Table 2. Linear Correlation Coefficient for Turbulence and Radar Echo Characteristics

Turbulence Measurement	Echo Characteristic	Correlation Coefficient 1964	Correlation Coefficient 1965
$\sigma(U_{de})$	$Z_{e(max)}$ (of storm)	0.514	0.516
$\sigma(U_{de})$	$Z_{e(max)}$ (of storm)		0.220
$\sigma(U_{de})$	Z_e gradient$_{(max)}$ (along flight path)	0.322	0.194
$\sigma(U_{de})$	Z_e gradient$_{(ave)}$ (along flight path)	0.315	- 0.092
$U_{de(max)}$	$Z_{e(max)}$ (of storm)	0.464	0.329
$U_{de(max)}$	$Z_{e(max)}$ (along flight path)		0.068
$U_{de(max)}$	Z_e gradient$_{(max)}$ (along flight path)	0.302	0.091
$U_{de(max)}$	Z_e gradient$_{(ave)}$ (along flight path)	0.241	0.226

Severe turbulence encounters outside the core areas were as frequent in 1965 as in 1964. This sustains the earlier concept [1] that severe turbulence is widely distributed in storms whenever the core Z_e indicates damaging hail (Z_e = $10^5/mm^6/m^3$). Figure 1 shows a flight on May 25, 1965. The main core of the storm with $Z_e = 2.5 \times 10^5 mm^6/m^3$ was 12 n. mi. west of the flight path. For this flight (U_{de}) max is 34 ft. per sec. and $\sigma(U_{de})$ is 8.97. The British Scimitar aircraft flying the same pattern on this occasion experienced similar turbulence.

Figures 9 and 10 show the distributions of derived gust velocity recorded during the 1964 and 1965 seasons. The data indicate lower frequency of extreme turbulence at the higher altitude. The frequency of moderate turbulence (U_{de} 35 ft. per sec.) is about the same at 27,000 and 37,000 ft.

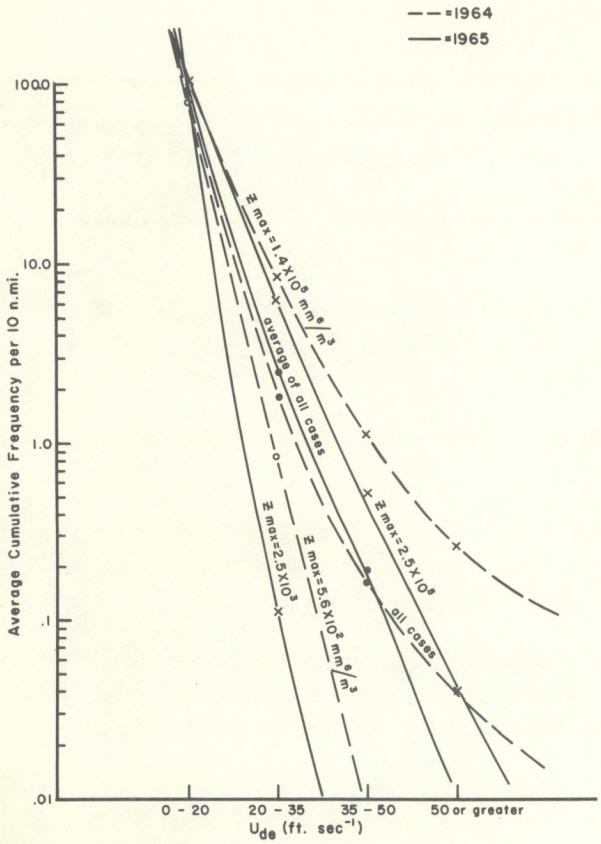

Fig. 9 - Average cumulative frequency of derived gust velocities per 10 n. mi. of flight in thunderstorms for representative values of maximum radar reflectivities (Z_e) of storm cores.

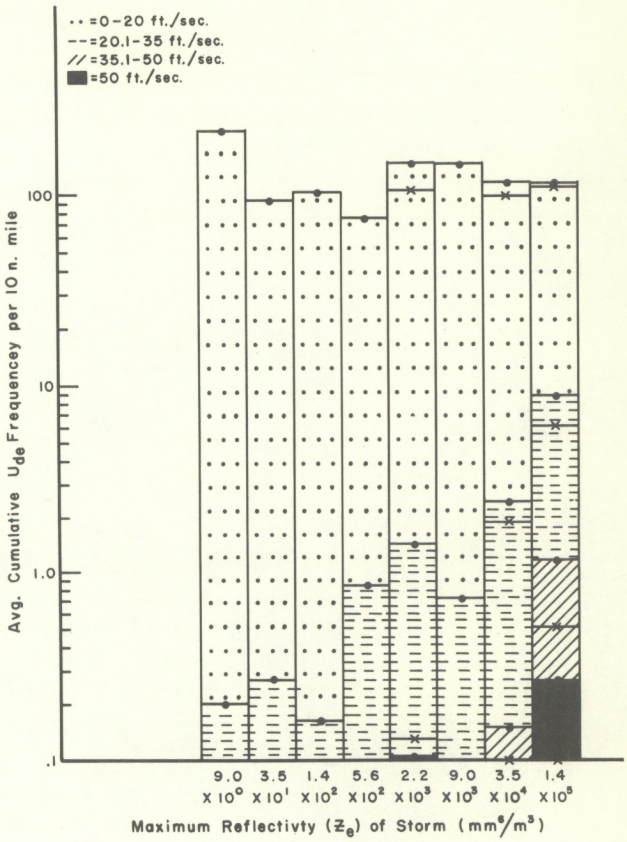

Fig. 10 - Average distribution of derived gust velocities per 10 n. mi. of flight in thunderstorms for 1964 and 1965.

4. SUMMARY

The 1965 data support the conclusions of earlier studies. The maximum reflectivity (Z_e) of the storm is the most reliable indicator of turbulence in thunderstorms. Moderate to severe turbulence may be encountered 10 to 15 miles from the center of storms whenever the maximum reflectivity is 3.5 x $10^4 mm^6/m^3$ or more. The frequency of severe and extreme turbulence seems slightly diminished at higher altitudes.

REFERENCES

1. Lee, J. T., "Thunderstorm Turbulence and Radar Echoes 1964 Data Studies," ESSA Technical Note 3; NSSL Report 24, 1965, pp. 9-28.

2. Lhermitte, R. M. and E. Kessler, "A Weather Radar Signal Integrator," NSSL Tech. Memo No. 2, 1965, 8 pp.

3. Gray, K. C. and K. E. Wilk, "Data Processing at NSSL in 1964," ESSA Technical Note 3, NSSL Report 24, 1965, pp. 111-121.

4. Battan, L. J., Radar Meteorology, University of Chicago Press, 1959, 161 pp.

5. Wilk, K. E. and S. M. Kulshrestha, "Wave Length Dependence of the Radar Reflectivity of Water and Ice Spheres," ESSA Technical Note 3; NSSL Report 24, 1965, pp. 33-34.

6. Miller, E., "1964 Rough Rider Summary of Parameters Recorded, Test Instrumentation, Flight Operation and Aircraft Damage," Aeronautical Systems Division Technical Report ASD-TR-65-1, 1965, 40 pp.

7. Pratt, K. G. and W. G. Walker, "A Revised Gust-Load Formula and a Re-evaluation of V-G Data Taken on Civil Transport Airplanes from 1933 to 1950," National Advisory Committee of Aeronautics Report No. 1206, 1954, pp. 1-4.

8. Lappe, O., "A Preliminary Evaluation of the F-100 Rough Riders Turbulence Measurement System," Final Report on ESSA Contract W66-170, 1966 (to be printed in NSSL report series).

9. Kessler, E., and J. A. Russo, Jr., "Statistical Properties of Radar Echoes," in Proceedings 10th Weather Radar Conf., Wash., D. C., 1963, pp. 25-33.

SOME PHYSICAL AND DYNAMICAL ASPECTS OF A SEVERE RIGHT-MOVING CUMULONIMBUS

James C. Fankhauser
National Severe Storms Laboratory

ABSTRACT

The morphology and dynamics of an isolated severe thunderstorm are analyzed and interpreted using observations obtained by instrumented aircraft and radar. Several aspects of the Severe-Right (SR) quasi-steady-state thunderstorm model proposed by Browning are supported by features of the storm's motion pattern, RHI radar profiles, and by certain kinematic properties. Net cyclonic circulation measured near the cloud base is considered as a mechanism for steering the storm. Comparison of rainfall with low-level moisture convergence reveals that about 60% of the intercepted water vapor is deposited on the ground during the storm's persistent phase.

1. INTRODUCTION

Soundings by aircraft of convective storm environments have contributed fundamentally to our knowledge of storm dynamics (see Byers and Braham [4], Staff members, NSSP [15]). However, the full character of physical processes near and within cumulonimbus clouds is not well-known, and careful observations are still greatly needed. This paper presents an analysis of data collected near an isolated Cb on June 1, 1965, by two DC-6 aircraft operated as part of the NSSL observational program. During the aircraft investigations the radar precipitation echoes were constantly monitored by the NSSL WSR-57 radar.

2. SYNOPTIC SITUATION, CLOUD FEATURES, AND STORM MORPHOLOGY

Convergence along the dry front shown in figure 1(a) was enhanced by the orographic lift given to the moist air by the "Cap Rock" escarpment in the Texas panhandle (see topographic contours in figure 3).[1] These effects apparently combined to produce an initial precipitation echo on the NSSL WSR-57 radar at 1340 CST. During the following 30 minutes a thunderstorm grew as shown by photographs in figure 2. These photographs were taken from one of the investigating aircraft flying on a heading of 270° toward the southwest sector of the storm and they indicate the well-organized nature of the visual cloud. The storm system developed in a wind regime with typically pronounced vertical shear, and persisted nearly 5 hours. Its

[1] A vertical wind component of nearly 10 cm sec^{-1} is associated with horizontal winds of 10 m sec^{-1} lifted by an incline of 1000 ft. in 20 n. mi.

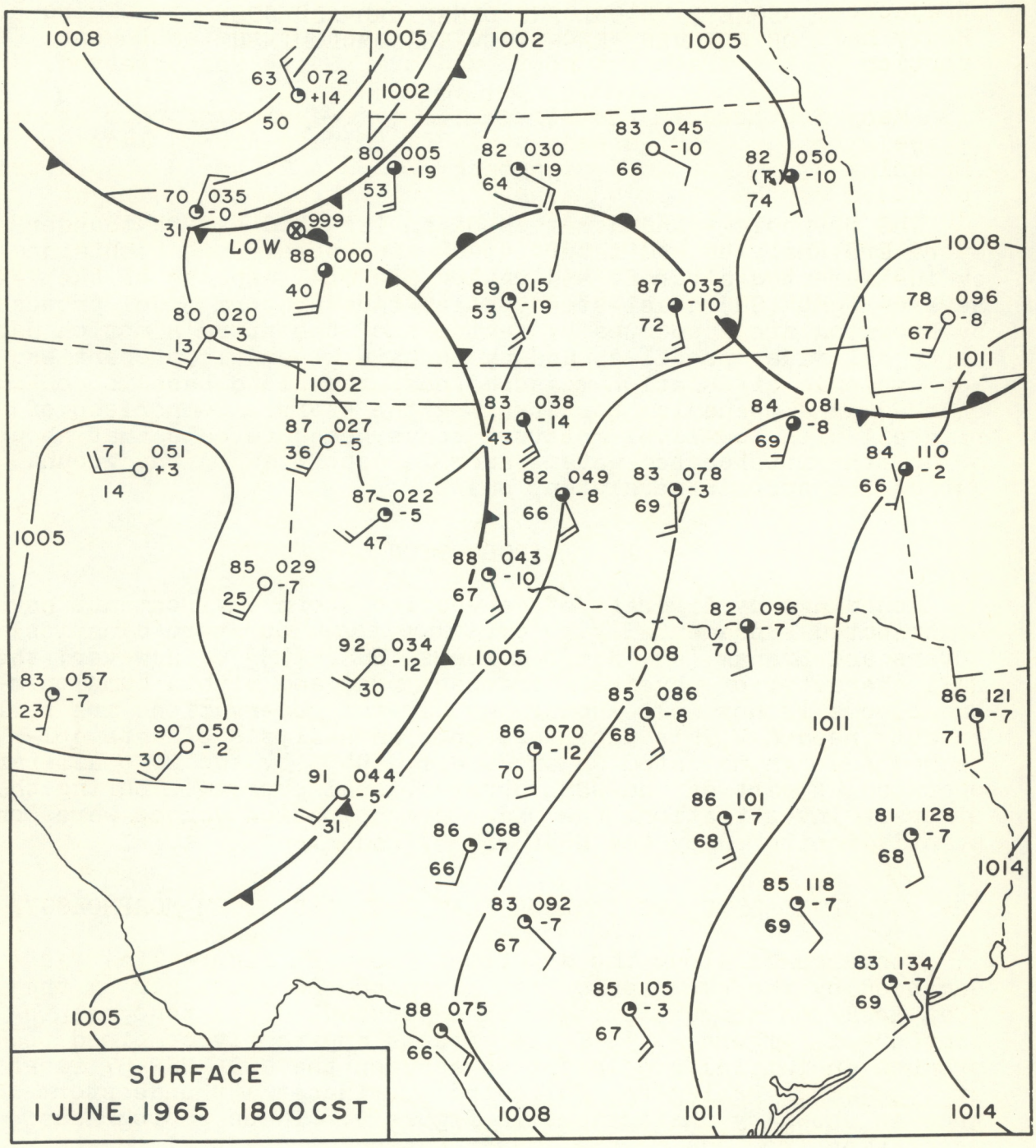

Figure 1a. Surface analysis, 1800 CST, June 1, 1965.

trajectory and evolution as a radar echo is shown in figure 3. Heavy hail damage was reported along much of the east-west portion of the track but no tornadic activity was observed.

Many features in the structure and behavior of this storm agree with the quasi-steady-state SR (Severe-Right) model of Browning [3]. The most prominent of these is the S-shaped track produced by the storm's rather sudden veering to the right during echo development and turning to the left shortly before dissipation. The hodographs shown in the inset of figure 3 illustrate that during much of the storm's lifetime it traveled to the right of the winds at all levels.

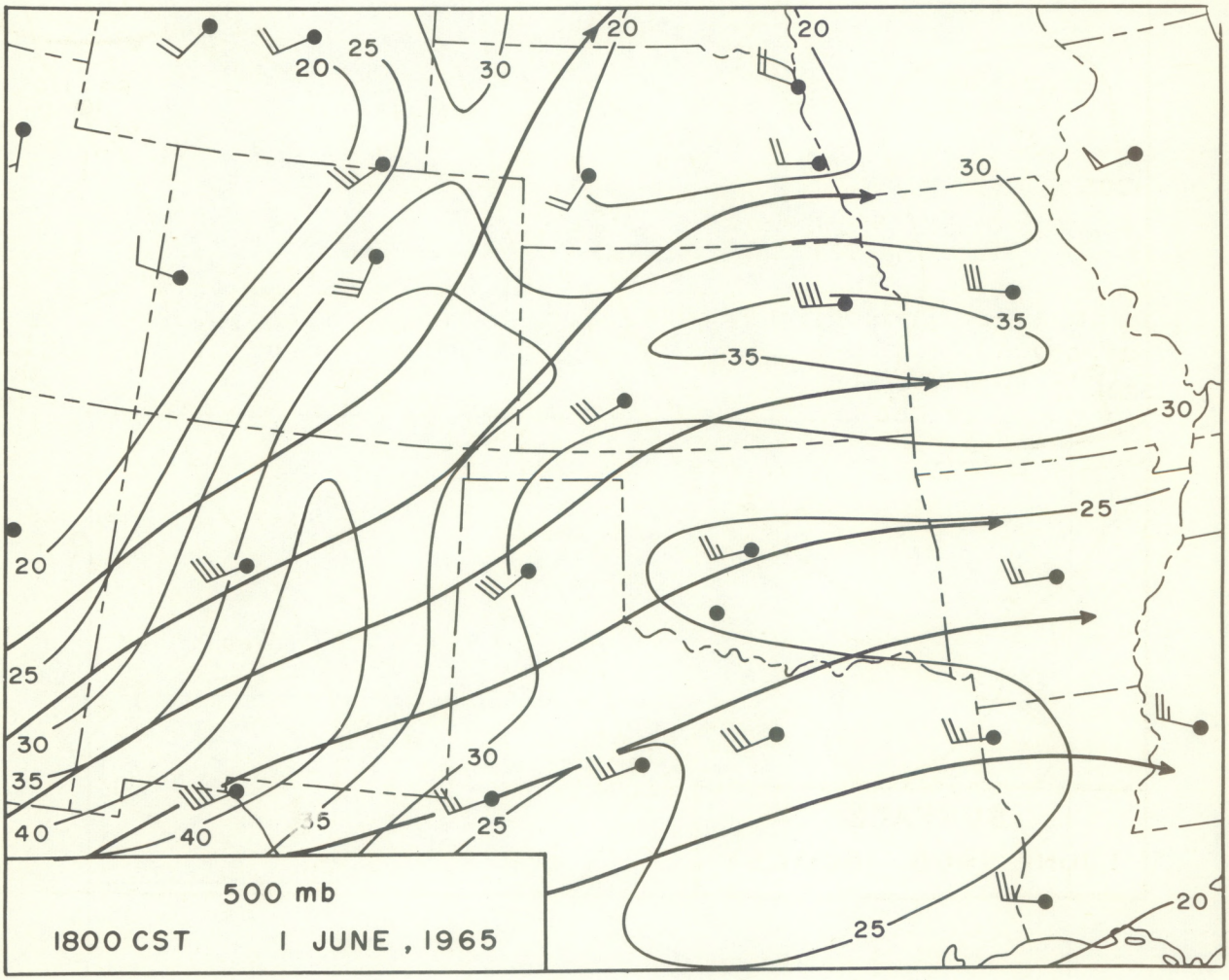

Figure 1b. 500-mb streamlines and isotachs in knots, 1800 CST, 1 June 1965.

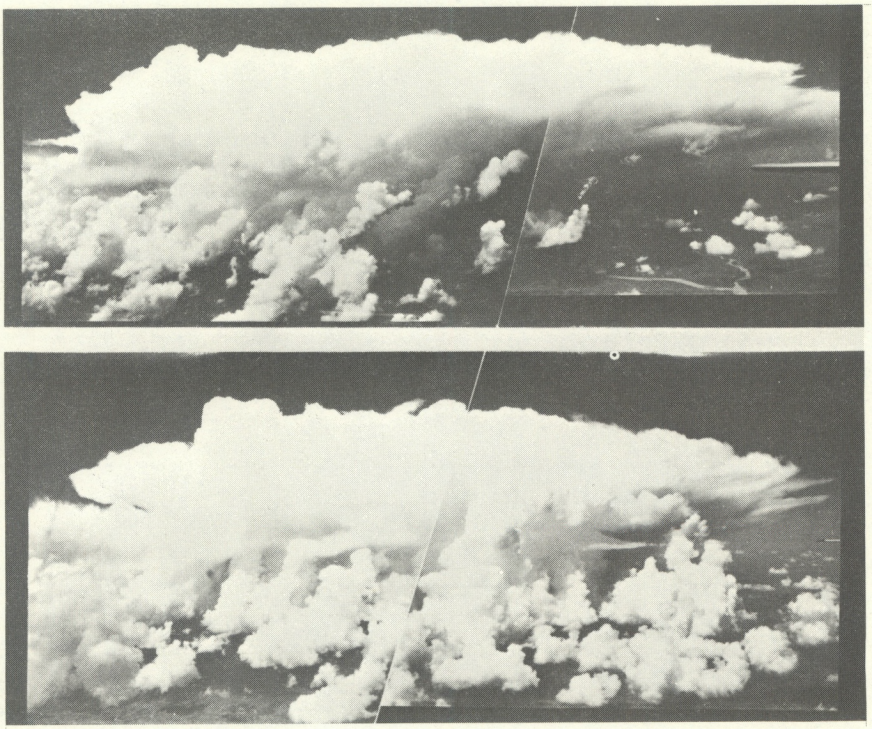

Figure 2. Photographs taken from aircraft at 18,000 feet on 270° heading about 1415 CST, approximately 50 n. mi. ESE of cloud (see figure 3).

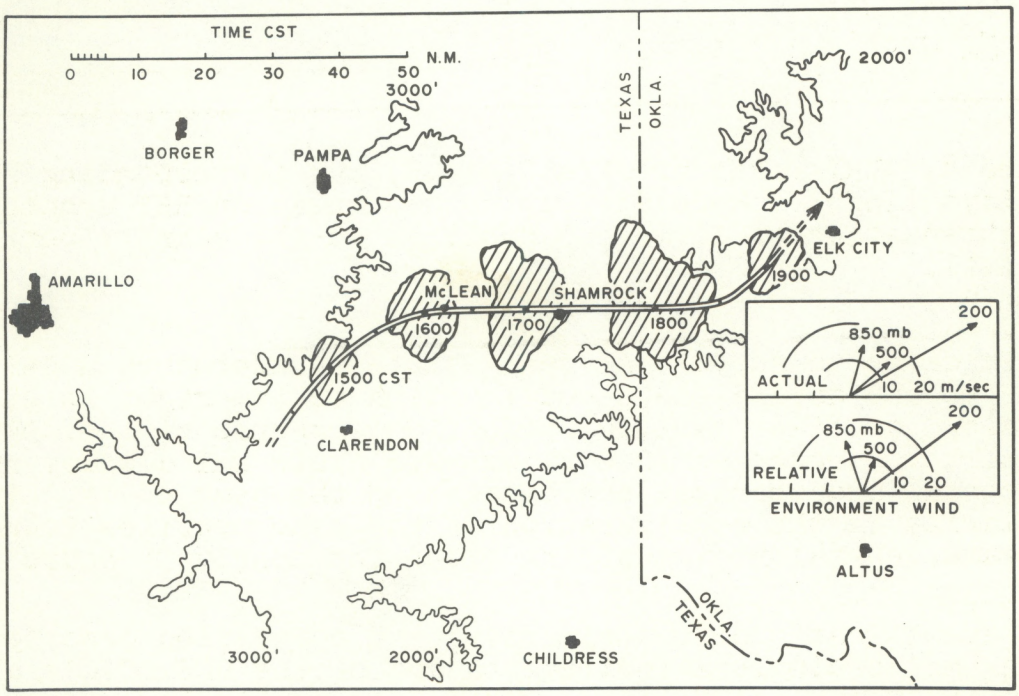

Figure 3. PPI radar echo trajectory and 1800 CST wind hodographs, June 1, 1965. Hourly echo configuration shown by hashing. 30-minute displacement indicated on track.

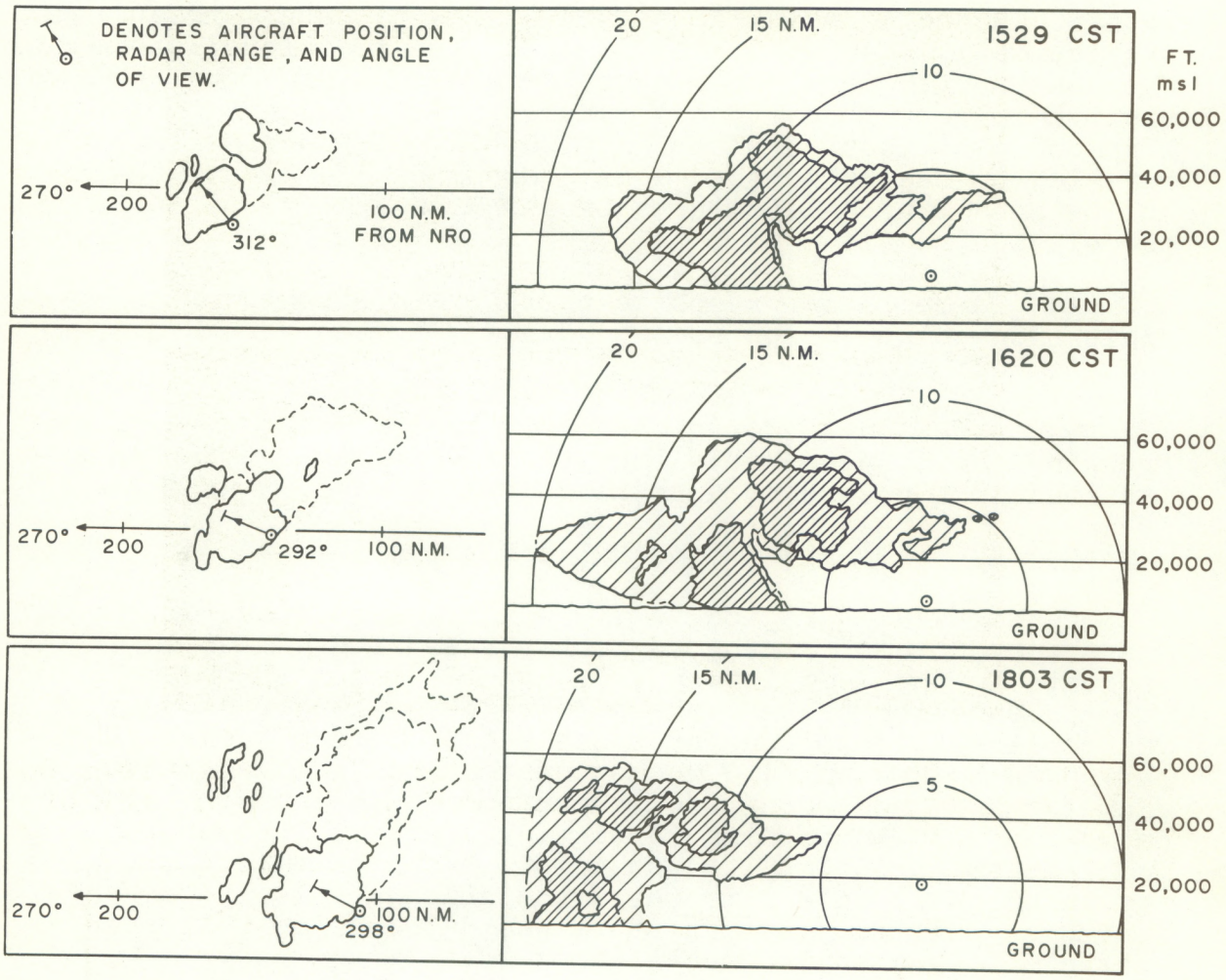

Figure 4. RHI radar profiles (right) and corresponding PPI displays (left). More densely hashed areas on RHI denote signal attenuation of 16 db. Dash lines on PPI signify outline of anvil.

Evidence to support a steady-state thunderstorm model just prior to and during the cloud's motion to the right is given by RHI cloud profiles derived from filmed records of the RDR-1D RFF airborne radar.[2] (See figure 4.) This RHI display shows horizontal and vertical coordinates on the same scale. The similarity in the configuration of the echo profiles found in the same general region of the cloud for nearly $3\frac{1}{2}$ hours is

[2]The specifications for this radar and a detailed description of the meteorological instrumentation on the RFF DC-6's are given in "Manual of Meteorological Instrumentation and Data Processing," by Carl M. Reber and Howard A. Friedman, Research Flight Facility, ESSA, Miami, Fla.

rather convincing evidence that the flow patterns are at least statistically steady with time. A three-dimensional storm model was constructed from radar cross sections obtained by the investigating aircraft during one complete circuit about the storm. The echo distribution shown in figure 4 and the organization revealed by the referenced model (not shown) agrees with the following additional features of the Browning [3] steady-state circulation model:

(1) There is an extensive overhang in advance of the precipitation column which slopes downward to the ground toward the storm's left flank;

(2) A region of lower reflectivity (called the vault by Browning) which penetrates into the core of the storm beneath its highest top; and to a small degree,

(3) A hook-shape in the PPI echo display.

If the "vault" region is viewed as the location of an organized updraft as Browning suggests, the RHI profiles in figure 4 indicate further consistency with the SR model in that the echo-free indentation tilts upshear from the region of cloud entry. The configuration of updrafts has recently been treated theoretically by Newton [12] who shows that for a given draft diameter and shear condition the slope in the upshear sense decreases with increasing vertical velocity. The echo wall is steepest at 1529 CST (just prior to the storm's veering to the right). At this time the translational velocity of the storm is a minimum and the storm would behave most like an obstacle to the environmental flow.

In accordance with the hypothesis of Newton and Fankhauser [13], the areal growth of the echo after turning to the right corresponds to its greater velocity relative to the moist air at low altitudes. While some of this deviation to the right of the upper winds may be explained by recurrent growth on the storm's right flank, careful analysis of the PPI data reveals that this explanation is insufficient. A net cyclonic circulation was measured by the aircraft in the low levels of the near-cloud environment and it is shown in Section 4 that a storm-environment interaction similar to the hydrodynamic Magnus effect [5,9] might have contributed to the storm's motion to the right of the ambient flow.

3. KINEMATIC PROPERTIES OF THE NEAR-CLOUD ENVIRONMENT

Wind data obtained from the Doppler navigational system aboard the RFF DC-6's are a basis for evaluation of some mesoscale kinematic properties of the atmosphere surrounding the storm. To obtain a consistent measure of the air flow with respect to the cloud system, each aircraft observation is

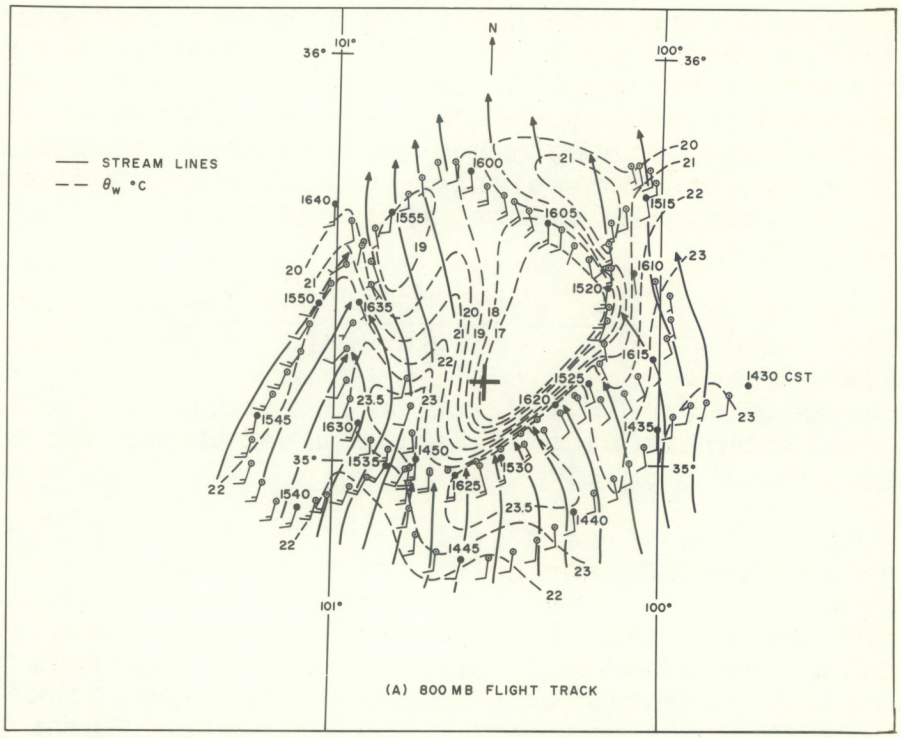

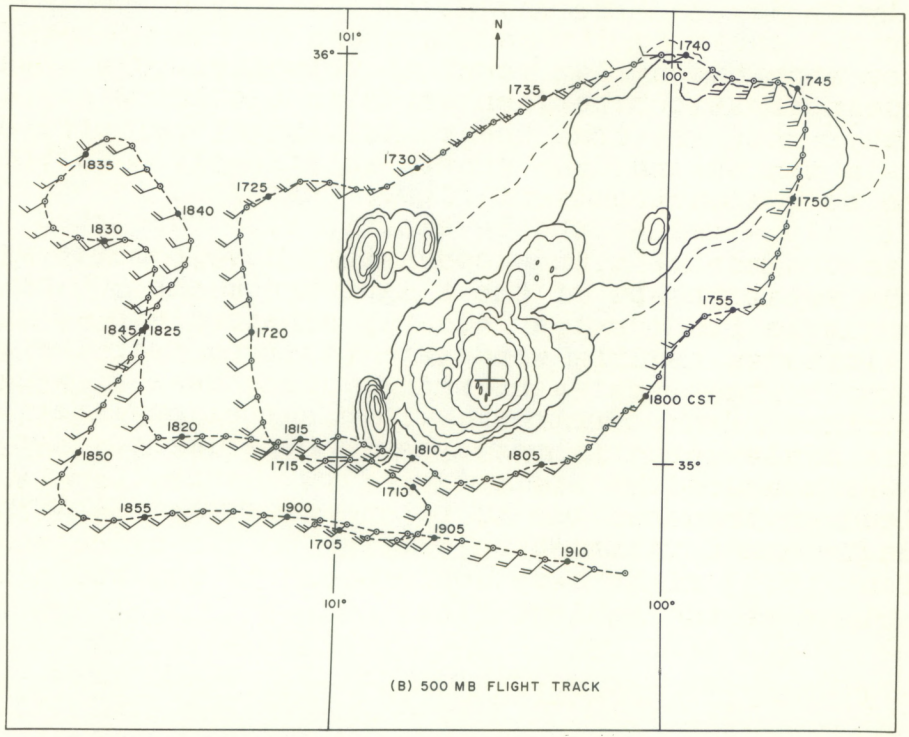

Figure 5. Aircraft flight data relative to radar echo centroid (bold cross). (a) 800-mb track, winds, streamlines, and wet-bulb potential temperature, (b) 500-mb track and winds. Radar echo outline and 6-db intensity contours derived from NSSL WSR-57 PPI display at 1630 CST.

positioned in a coordinate system with the cloud centroid at the origin. Figure 5 shows the adjusted low- (≈800 mb or 6,400 ft.) and high- (≈500 mb or 18,250 ft.) level flight tracks relative to the cloud and the winds at 1-minute intervals. Wind data are obtained at 10-second intervals; however, a 50-second non-weighted running mean is systematically applied using the smoothing function:

$$\overline{W} = \frac{W_{i-2} + W_{i-1} + W_i + W_{i+1} + W_{i+2}}{5} \qquad (1)$$

where i-intervals are 10 sec. With an average air speed of 240 kts. the aircraft displacement equivalent to the smoothing interval is about 3 n. mi.

The flow at both levels is generally similar to that prescribed by Fujita and Arnold [6] for an isolated Cb over Kansas. Cyclonic curvature and streamline confluence are detectable at the cloud base near the cloud's right-forward flank. Water vapor concentrations in the same region (see θ_W in figure 5a) suggest an organized region of inflow. The absence of well defined outflow in the pattern of winds measured near the base of the storm also agrees with analyses by Fujita and Arnold [6] and by Fujita and Byers [7].

Newton and Newton [14] found it convenient, in treating the dynamical interactions between large cumulonimbus and environments with strong vertical shear, to regard the vertically mixed momentum in the up and down drafts as effectively creating a solid obstacle to the ambient flow. That this is approximately so, especially at mid-cloud levels, is also supported by analysis [6, 8]. Because of new convective developments upstream and the irregular shape of the flight track the 500-mb winds shown in figure 5b do not so clearly substantiate an obstacle effect. However, maximum winds are observed near the right and left flanks of the radar echo while local areas of weaker winds appear upstream and downstream. This agrees qualitatively with observations made during hydrodynamic experiments involving solid cylinders in quasi-potential flow. (See [10], pp. 154-156.) Further implications of storm-environment interactions are amplified in section 4.

Figure 5a shows the adjusted low-level flight track flown between 1430 and 1640 CST. There are three nearly complete circuits around the cloud at this level. Overlapped data from successive circuits provide three independent evaluations of the net circulation, divergence, and relative vorticity near the storm at 800 mb. A single estimate of the same quantities is provided by the circuit flown at 500 mb. For the computations, the following analytical expressions are used:

Relative Circulation: $\Gamma = \Sigma\ \bar{v}_t\ \Delta\ L$ (2)

Divergence: $\bar{D} = 1/A\ \Sigma\ \bar{v}_n\ \Delta\ L$ (3)

Relative Vorticity: $\zeta = \Gamma/A$. (4)

Summation around a closed circuit of length, L, and area, A, is denoted by Σ and $\bar{v}_n$ and $\bar{v}_t$ represent, respectively, the normal (positive when directed outward) and tangential (positive when cyclonic) components of the average wind along a segment $\Delta L = c\ \Delta t$. The aircraft ground speed is c and steady-state conditions are assumed to prevail within L.

Table 1 lists results of the computations. The temporal variations of the quantities measured at 800 mb are of particular interest. Circulation, tangential velocity, and thus relative vorticity are cyclonic and largest for the period centered on 1545 CST (just before the storm veers to the right), but diminish significantly thereafter.

Table 1

Summary of Kinematic Properties

Time		1545	1600	1615	1745
p	Mean flight-level pressure, [mb].	800	800	800	500
A	Area of circuit, [$10^9 m^2$].	5.8	6.3	4.9	12.2
L	Length of boundary, [km].	306	330	280	446
$\bar{r}$	Mean circuit radius, [km].	43	45	40	62
Γ	[$10^4 m^2 sec^{-1}$].	18.0	10.6	4.5	-3.8
$\bar{D}$	[$10^{-4} sec^{-1}$].	-1.2	-1.6	-1.7	-0.8
ζ	[$10^{-5} sec^{-1}$].	3.1	1.7	0.9	-0.3
$\bar{v}_n$	Mean radial component, [m sec^{-1}].	-2.2	-3.1	-3.0	-2.2
$\bar{v}_t$	Mean tangential component at radius, $\bar{r}$, [m sec^{-1}].	0.6	0.3	0.2	-0.1

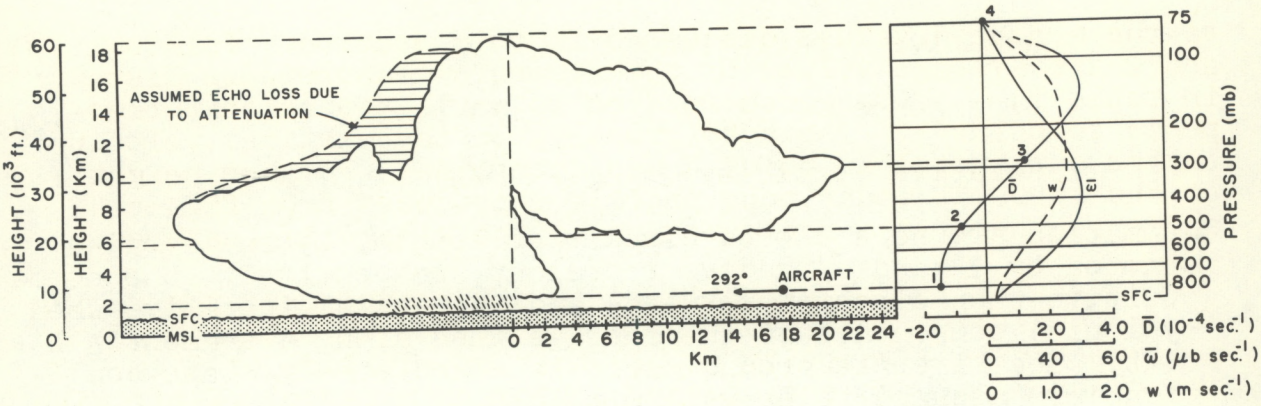

Figure 6. Mesoscale divergence and vertical velocity profiles (right) derived from measurements near a thunderstorm whose RHI profile is shown at a common height scale (see text).

The net convergence and storm size, in contrast to the rotational aspects, increase markedly after the storm track assumes a more easterly course. Growth of the storm after veering to the right reflects its greater velocity relative to the moisture laden low-level air.

The horizontal mean divergence, $\bar{D}$, in the upper regions of the cloud was estimated from the expansion of the radar echo produced by the anvil "blow-off" (see figure 4). In the practical evaluation we consider $\bar{D} = (1/A)(dA/dt)$, where A is the mean anvil area at the middle of the cloud's life history, and ΔA is measured during the time interval Δt between successive radar presentations ($\approx$7 to 10 minutes). The radar cross section shown in figure 6 places the leading edge of the anvil at 32,000 ft., or 280 mb. The average divergence indicated for this level during a period when radar echoes indicate steady cloud circulations is 1.3×10^{-4}/sec.[3] This compares closely in magnitude to calculations at low levels where the sign is compensating. As might be expected, horizontal divergence at 500 mb, tabulated in table 1, is negative (convergent flow), but nearly an order of magnitude smaller than values measured at cloud base and anvil levels.

The right-hand portion of figure 6 shows the vertical profiles of horizontal divergence, $\bar{D}$, and associated kinematic vertical velocity, expressed in both pressure and height coordinates, which are derived from the simplest interpretation

[3]This is likely to be an underestimate because of subsidence and evaporation of radar reflecting hydrometeors.

of the measured values discussed in this section. Points 1 and 2 are average values of the aircraft measurements listed in table 1; divergence related to anvil expansion corresponds to point 3. The zero crossing on the vertical velocity curves designated as point 4 was determined from the height of the 1620 CST radar echo profile reproduced from figure 4 and shown here at a scale common to the kinematic features.

An evaluation of synoptic-scale divergence over the region of storm development leads by continuity to an estimate of the maximum vertical velocity (w_{max}) near an altitude of 5 km. On the other hand, buoyancy forces acting on a parcel of air with a wet-bulb potential temperature of 23°C would produce a maximum updraft near 200 mb or 12 km. In the broad scale environment w_{max} undoubtedly occurs at an altitude far below that corresponding to the level of updraft maximum within an active convective cloud, while the altitude where adiabatic vertical velocity reaches a maximum is probably too high, since such depleting effects as precipitation drag and entrainment are not considered in its evaluation. Therefore, the actual level within the thunderstorm where the net updraft achieves its peak could be expected to lie somewhere between 5 and 12 km. The agreement between this crude estimate for the altitude of w_{max} and that shown by the vertical velocity profiles in figure 6 is reasonably good.

Since visual cloud occupies only a fraction of the area enclosed by the flight track, L, it is unlikely that upward motion of the indicated magnitude is occurring uniformly everywhere within L. Rather, it is probable that the air converges from the radius of L toward the cloud under conditions which approximate a conserved mass flow rate, i.e., $v_n r$ = constant. With this condition, the radial inflow increases to 12 m sec^{-1} at a radius of 10 km (essentially that of the radar echo extending above the anvil level) and the associated convergence becomes 2.4×10^{-3} sec^{-1}. This is an order of magnitude greater than values measured across L, 40 to 50 km from the cloud, and should be reflected in a corresponding increase of vertical velocity over those values shown in figure 6.

If net draft velocities of tens of meters per second are actually attained over large regions within the cloud, then significant differences undoubtedly exist between in-cloud and ambient horizontal air motions. Large differential velocity could account for both the presence of an effective obstacle and the inertial resistance it presents to the environmental flow. The implications of these possibilities are expanded in the following section.

4. STORM MOTION IN RESPONSE TO POSSIBLE STEERING FORCES

It is of interest to inquire at this point concerning observed deviations in the storm's path in relation to hydrodynamic interactions between the cloud circulations and the ambient flow. Principles involved may be analogous to those attending the Magnus effect where, ideally, a horizontal orthogonal deflecting force, F, is generated on the surface of a solid cylinder rotating in uniform fluid flow according to

$$F = -\rho V_r \Gamma \quad . \tag{5}$$

In equation (5) F is the force per unit height of the cylinder, ρ the ambient fluid density, V_r the velocity of the flow relative to the cylinder, and Γ the circulation at the boundary. Deflection force expressed in this manner is the simplest form of the general equations of Kutta and Joukowski for lift due to circulation. It is clear that a deflecting force depends on the combination of relative velocity and circulation -- if either is zero there can be no deflection. A noteworthy result of the more general equations of Kutta-Joukowski is that the existence of a deflecting force is independent of the shape of the rotating element. (See [10], p. 192.)

For the purpose of further discussion a simple model of thunderstorm circulation is adopted wherein a steady net updraft converges to a level of maximum vertical velocity within the storm. Most of the convected air originates in the moist subcloud layer and possesses horizontal momentum which is small compared to that of the air throughout the depth of the cloud-bearing environment. As the inflow air rises in the updraft it presents inertial resistance to the ambient flow at any level. The level where the convective column acts most like an obstacle should therefore correspond to the region where vertical transport of low-level momentum is occurring most rapidly; i.e., the level of maximum updraft velocity.

If the air entering the updraft possesses a rotational component, its rotation should, as a result of vertical stretching, increase while the air ascends to the level of maximum updraft velocity. Thus two factors essential to the existence of the Magnus effect may act most favorably at the same cloud level; (1) relative velocity resulting from the inertial resistance produced by the vertical transfer of momentum, and (2) circulation of the draft boundary.[4]

---

[4]Since the general theoretical treatment of Kutta-Joukowski is based on incompressibility, the tendency for the environment to be non-divergent near the level of maximum draft velocity may be another condition favoring the formation of a significant horizontal force.

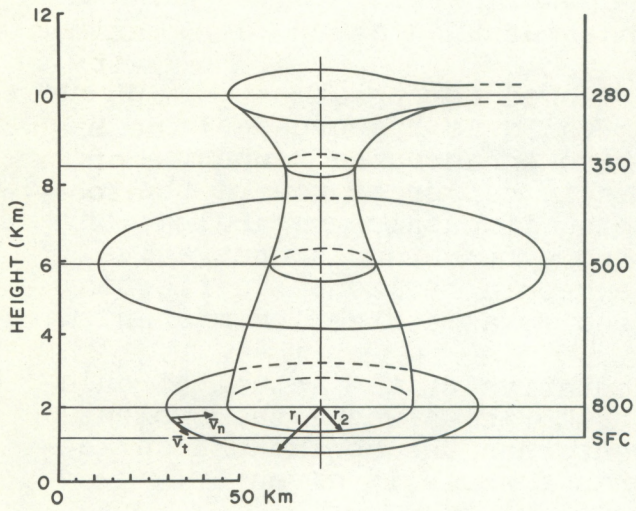

Figure 7. Idealized schematic representation of thunderstorm radar echo and mean flight track radii. (For explanation of symbols and further discussion, see text.)

Earlier speculation noted that winds measured at 500 mb, where significant storm-environment reactions are most likely, were disturbed by complicating convective developments up- and downstream. Large convergence values at 800 mb (see table 1) suggest that a major portion of air at that level is entering the cloud circulation. Therefore, hydrodynamic properties which could produce steering forces are probably not effective at that altitude. However, the circulation computed from 800-mb winds may be used to estimate the rotation at the cloud boundary aloft.

Absolute circulation, Γ_a, at the flight track radius, r_1, (see figure 7) may be expressed as the sum of the relative circulation Γ listed in table 1 and the contribution of the earth's rotation;

$$\Gamma_a = \Gamma + f A_1 \quad , \tag{6}$$

where A_1 is the area of a circle with radius, r_1, and f is the Coriolis parameter.

If the atmosphere at r_1 is considered to be essentially barotropic, then by Bjerknes circulation theorem $d\Gamma_a/dt = 0$ and Γ_a will be conserved as the air converges to r_2, the radius of the PPI echo.

To estimate the tangential velocity $\bar{v}_{t_2}$ at r_2 we note that

$$\Gamma_a = \Gamma_1 + f A_1 = \Gamma_2 + f A_2 = 2\pi \bar{r}_2 \bar{v}_{t_2} + f(\pi \bar{r}_2^{\,2}) \tag{7}$$

and derive the expression of $\bar{v}_{t_2}$;

$$\bar{v}_{t_2} = \frac{\Gamma_a - f(\pi \bar{r}_2^{\,2})}{2\pi \bar{r}_2} \quad , \tag{8}$$

where $\Gamma_a = 64 \times 10^4 m^2 sec^{-1}$ (a constant from equation (6)), $\bar{r}_2 = 24$ km, $f = 0.8 \times 10^{-4} sec^{-1}$, and the bar notation denotes mean values. Substitution yields a result which indicates an

increase in tangential velocity from 0.6 m sec^{-1} at $\bar{r}_1$ to 3.3 m sec^{-1} at $\bar{r}_2$. Relative circulation, Γ_2, associated with this velocity is 50 x $10^4 m^2 sec^{-1}$ or approximately 3 times greater than Γ_1 associated with the winds measured at $\bar{r}_1$.

The barotropic assumption invoked for treatment of circulation undoubtedly becomes less valid as r decreases; however baroclinic effects may well act to enhance the tangential velocity component of the air as it converges toward the cloud. In light of this and the foregoing discussion regarding convergence in the updraft, Γ_2 probably represents a conservative estimate for circulation aloft where a horizontal deflecting force is likely to be most effective as a steering mechanism.

If Γ_2 is considered representative of the actual circulation near the cloud boundary at the level where the ambient flow is essentially non-divergent, then the horizontal deflecting force acting on the storm as a whole is given by

$$\mathbb{F} = -\bar{\rho}_h \bar{V}_r \Gamma_2 h \quad , \tag{9}$$

where h represents the depth through which the cloud presents an effective obstacle to the flow. For the purpose of evaluation, the following values are adopted from observed conditions: h = (10-6) km = 4 x 10^3m (a region in the near-cloud atmosphere possessing small horizontal and vertical shear), $\bar{\rho}_h$ = 0.5 kg m^{-3}, and $\bar{V}_r = |\bar{\mathbb{V}}_h - \mathbb{V}_s|$ = 12.5 m sec^{-1}, where $\mathbb{V}_s$ = 265°/8 m sec^{-1} and $\mathbb{V}_h$ = 237°/19 m sec^{-1} are the storm and ambient air velocity vectors, respectively, and the bar notation denotes means for the depth, h. Substitution leads to a deflective force of 1.25 x 10^{10} kg m sec^{-2}.

The form drag exerted on the same cloud section can be estimated from

$$\mathbb{D} = C_D h \bar{r}_2 \bar{\rho}_h \bar{V}_r^2 \quad . \tag{10}$$

Fujita and Grandoso [8] used aircraft winds to arrive at a drag coefficient, C_D, of approximately 1.0 near a well-organized isolated thunderstorm similar to the one described here. If this value is used with the other defined terms, the drag force tending to accelerate the storm in the direction of V_r (220°) is computed to be 0.75 x 10^{10} kg m sec^{-2}. The sum of orthogonal drag and deflection force vectors is directed from 275°; within 10° of the motion during the period when quasi-steady circulations seemed to prevail.

A review of the storm's morphology as depicted in figure 3 seems appropriate in terms of the possible forces governing the motion. The first radar echo appeared over an area where complementary kinematical and mechanical convergence mechanisms

were present; specifically, the eastward moving dry line and the Cap Rock land form of the Texas Panhandle. In stages of early growth its motion corresponded closely to the winds in the mid-troposphere. When convergence near the cloud base was increasing (see table 1 and figure 3) the echo path was gradually deviating to the right of the winds. This turning can be viewed as a response to a horizontal deflecting force acting on a rotating updraft whose circulation is increased by convergence.

During the period from 1600 to 1830 CST a balance may have existed among forces owing to form drag, rotation, and inertial resistance since the storm velocity is nearly constant during that time. The observed motion back to the left after 1830 CST may have occurred because rotational properties required to maintain the Kutta-Joukowski deflection force were no longer present in the air mass feeding the storm. Reasons for this loss could result from changes in the character of the synoptic scale flow or to changes in the slope of terrain over which the storm moved. Note the correspondence between the deviation to the left and the storm's passage across the 2000 ft. topographic contour into a region of considerably flatter terrain. From the standpoint of mass continuity, the rapid storm decay after its turn to the left may be explained in terms of diminished relative low-level inflow.

5. MOISTURE AND ENERGY BUDGET CONSIDERATIONS

One of the most complete analyses of thunderstorm water and energy budgets based on observational data was produced by Braham [2]. His data and conclusions pertain primarily to small and short-lived thunderstorms, and indicate that only about 10% of the water vapor entering the clouds is eventually measured as precipitation at the ground. Considerable evidence collected in recent years suggests that the large severe storms of the Great Plains are far more efficient in converting intercepted water vapor into rainfall. Newton [11] assessed the continuity of water substance in an Ohio squall line, and found that more than half of the water vapor converging into the convective circulation was measured as rain. In a more recent study of an Oklahoma squall line [12] he further concluded that "once a storm achieves the persistent phase, the amount of rain deposited at the ground is essentially equivalent to the water vapor convergence in low levels." He refers to squall line elements where smaller surface-to-volume ratios are associated with smaller dry air entrainment and evaporation at cloud boundaries than exists when convective clouds are isolated.

Studies of the moisture budget of individual isolated cumulonimbi are scarce and the detailed measurements available in the aircraft data afford an attractive means for evaluating the moisture balance of the storm under study. Variations in specific humidity around the cloud at low levels were estimated from

absolute humidity measurements provided by the infrared hygrometer. Moisture flux, M, into the region confined within the closed flight track, L, was numerically evaluated from

$$M = -\frac{\Delta p}{g} \sum \bar{v}_n \bar{q} \Delta L \qquad (11)$$

where Δp is a unit pressure depth of 1 mb, $\bar{v}_n$ is again the mean horizontal wind component normal to a segment ΔL, and $\bar{q}$ is the average specific humidity along ΔL.

Since an aircraft collects data at a single altitude at a particular time, extension of the results to three dimensions requires independent data or vertical extrapolation of the flight-level measurements. Examination of the distribution of wind and moisture profiles provided by the aircraft's climb from 800 to 500 mb, and by rawinsonde ascents made at Ft. Sill, Oklahoma, and Amarillo, Texas, revealed that the aircraft measurements at 800 mb were representative of mean inflow conditions and that the moist sub-cloud layer was about 200 mb thick.

When the water vapor convergence evaluated at 800 mb is applied to the layer of 200 mb depth lying immediately above the surface, the net moisture flux into the region beneath the storm near the beginning of its persistent stage becomes 28 kton sec^{-1} (2.8×10^7 kg sec^{-1}). This is two orders of magnitude greater than that determined by Braham [2] for small thunderstorms with average diameter of 8 km and about 3 times larger than Newton's estimate for a 20 km segment of an Oklahoma squall line [12].

Rainfall data were sparse in the region affected by the storm; however, quantitative precipitation estimates are provided by the radar reflectivity-rainfall rate (Z-R) relationship. The cloud was 150 n. mi. distant from the radar during the period of aircraft soundings. In order to compensate for the dependence of echo intensity on range, the exponent on r in the simplified radar equation[5] was adjusted upward to 2.29 as recommended in the empirical study by Baxter [1]. Based on the revised exponent, reflectivity factors for discrete intensity steps were used to determine the corresponding rainfall rates according to the relationship

$$Z = 200\, R^{1.6} \qquad (12)$$

---

[5]Radar reflectivity is defined as

$$Z = \frac{P_r}{P_t} \frac{r^2}{C},$$

where P_r is the power received, P_t, power transmitted, and C the radar constant.

PPI intensity contours from the NSSL WSR-57 radar were traced for every step-gain sequence spanning the lifetime of the storm. The areas of the various steps were determined with the aid of automatic chart readers, multiplied by their respective Z-equivalent rainfall rates, and then summed for each sequence to determine the average storm-wide precipitation rate.

Confidence in the (Z-R) approach is gained by reference to a comparison with actual observational data shown in figure 8. Maximum rates, as well as changes in rate, are well correlated with the highest reflectivity and strong reflectivity gradients. Rain depth of 1.52 in. (38.6 mm) was measured in the rain gage between 1542 and 1654 CST, for a mean hourly rate of 32.2 mm hr^{-1}. For the same period the average rate calculated from radar data is 34.6 mm hr^{-1}.

The variations in area, total rainfall output, and output per unit area, throughout the life cycle of the convective system are shown in figure 9. From 1600 to 1800 CST the area of the radar echo was fairly constant and agrees reasonably well with earlier discussions of the storm's persistent character. Although the radar echo area is nearly constant during its motion to the right of the winds, its rainfall output continues to increase until just prior to dissipation and turn back to the left. This compares favorably with the trend indicated by the low-level divergence data in table 1.

Table 2 lists point-to-point comparisons of the rainfall rate derived from the quantitative radar measurements with rates computed from equation (11), assuming all the converged vapor is condensed. Although the curves shown in figure 9 and the results presented in table 2 both display considerable scatter, there seems to be reasonable evidence that early in the persistent state the convective system was converting approximately 60% of the intercepted water vapor into rainfall at the ground.

The mass of water vapor, W, in a vertical column of air with horizontal cross-sectional area of 1 m^2 and depth, $\Delta p = p - p_o$ is given by

$$W = -\frac{1}{g}\int_{p_o}^{p} q\,dp \ , \qquad (13)$$

where q is the specific humidity. If the moist layer extending beneath the cloud is of uniform depth, $\Delta p = -200$ mb, and characterized by a mean specific humidity, $\bar{q} = 8$ g kg^{-1}; substitution in (13) indicates that a water vapor mass of 16 kg overlays a unit surface area.

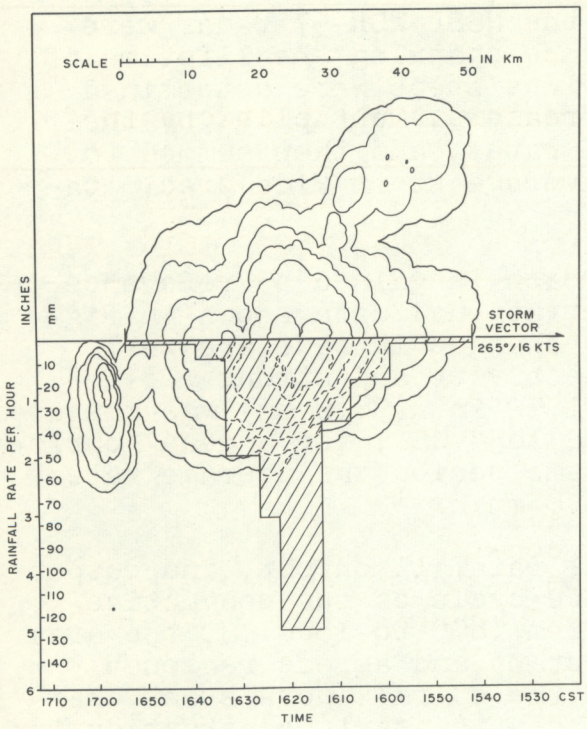

Figure 8. Rainfall rate (bar diagram) derived from recording rain gage located at McLean, Texas, (for position relative to storm trajectory, see figure 3) superimposed upon 6-db echo intensity contours at 1630 CST. $Z_{min} = 4.4 \times 10^2$ and $Z_{max} = 0.3 \times 10^6$ mm^6 m^3. Base rate profile also represents echo's path across rain gage.

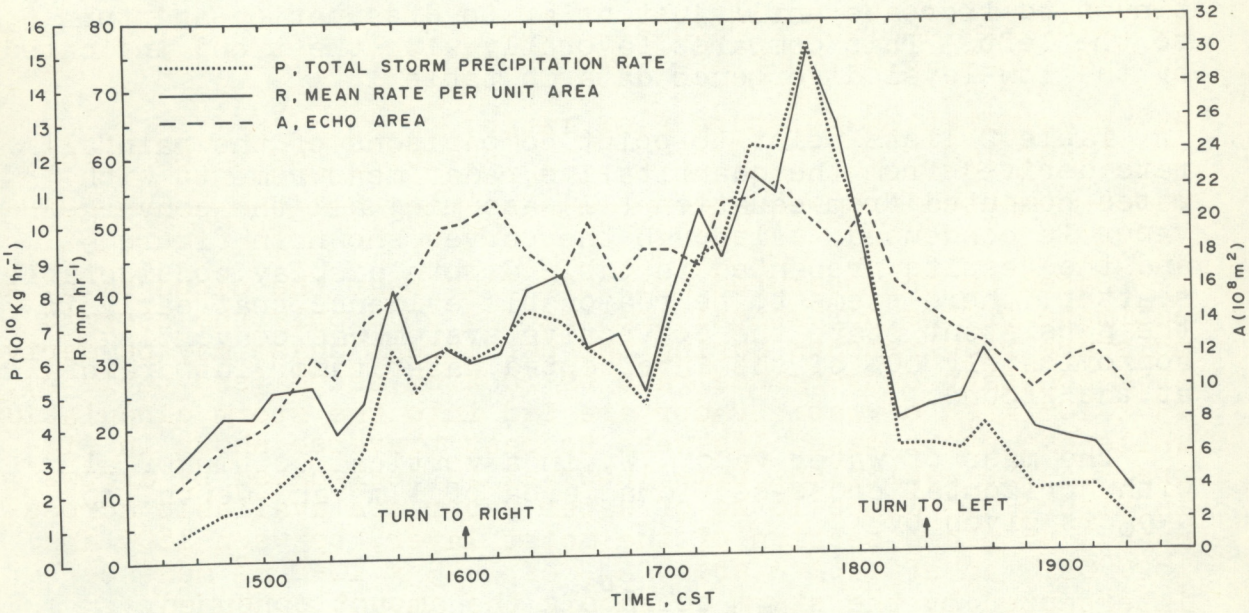

Figure 9. Time history of echo area, A_S, total liquid water precipitation rate, P, and precipitation rate per unit echo area, R, computed from Z-R relationship. Change in echo's translation is marked on abscissa.

Table 2

Summary of Moisture Flux-Precipitation Relationship

	Time (CST) 1545	1600	1615	Mean
a. Water vapor flux across vertical boundary surrounding the moist sub-cloud layer at flight track radius [kton sec^{-1}]	24	32	29	28
b. Equivalent precipitation rate at a point beneath the storm if all the converged water vapor is condensed and reaches the surface [mm hr^{-1}]	51	58	53	54
c. Liquid water output derived from quantitative radar measurements [kton sec^{-1}]	13	14	16	14
d. Average equivalent rainfall rate per unit radar echo area [mm hr^{-1}]	31	30	35	32
e. Precipitation-moisture flux ratio; (d/b) [%]	61	52	66	60

Based on the measured moisture flux near the cloud base, an estimate of the horizontal area needed to supply the storm's moisture requirements during the persistent phase may be derived. At a constant convergence rate of 28 kton sec^{-1} (see table 2), 23×10^4 kton of water vapor are fed into the storm circulation while the storm makes its west to east traverse shown in figure 3. The equivalent time interval is designated by arrows in figure 9. Since 16 kg of water vapor are available across each 1 m^2 plane section of the moist layer, between 1600 and 1820 CST, an effective area, A_r, of 1.45×10^{10} m^2 must be intercepted by the storm to supply the amount consumed. During the same period, an area, A_s, of 3.0×10^9 m^2 is swept by the traveling radar echo.[6]

[6]For a graphic interpretation of the relationship between a storm's path and its effective swath through the moist low-level air mass, see [13], figure 7.

The ratio A_r/A_s leads to the conclusion that, at any instant during the persistent stage, the areal extent of the air mass required to feed the storm is nearly 5 times larger than the storm itself. Because large isolated storms of the type analyzed here draw moisture from a considerable distance away, it follows that an air mass capable of producing localized severe convective activity is inherently limited in the number of storms it can sustain over a given geographic area.

Potential energy per unit time required to lift the mass of inflowing water vapor to the level of condensation is given by $\bar{M}\, g\, \Delta h$, where Δh is the lifting interval and $\bar{M}$ as given in table 2 is 28 ktons sec^{-1}. The storm profile in figure 6 indicates that the echo free region, presumed to be the updraft core, extends upward nearly 10 km. By regarding this height as the average level of condensation, the increment, Δh, with lower limit at the cloud base, may be taken as 8 km. With a steady rate of vapor influx of 28 kton sec^{-1}, the rate at which potential energy is expended due to ascent in the updraft is estimated to be 2.2×10^{12} joules sec^{-1}. Through latent heat release, continual condensation of all the water vapor entering the storm would make energy available at a rate of 70×10^{12} joules sec^{-1}.

Thus, the energy produced per unit time through the condensation process far exceeds that required to bring the inflow air to the point of condensation. Although energy provided by latent heat release is offset to some degree by such depleting effects as entrainment and re-evaporation, it appears from this analysis that sufficient residual energy exists to drive and sustain quasi-steady convective circulations as discussed in this paper.

6. SUMMARY

Aircraft and radar observations have been used to evaluate both directly and indirectly some features of the internal and near-cloud air motions associated with a large isolated thunderstorm. Kinematic properties of the adjacent environment, RHI profiles taken from airborne radar, and deviations in the storm track all support the premise that storms which move to the right of the upper winds have well-organized and persistent circulations. During growth, persistence, and dissipation the areal echo extent responds to changes in the relative low-level inflow. Convergence and divergence of equal magnitude are found at the inflow and anvil levels when radar indicates that the internal flow patterns are essentially steady. A restricted treatment of the circulation measured near the cloud base suggests that the storm's motion may have been influenced by its rotation. Radar precipitation measurements indicate that about 60% of the vapor converging toward the cloud at low levels was converted to rainfall at the ground.

In general, the results demonstrate the utility and reliability of aircraft data in the investigation of severe thunderstorms and the interpretive advantage gained by combining these measurements with ground-based observations. Uncertainties involved in the treatment of the cloud's rotational properties lead to the suggestion that instrumented aircraft flown at a common altitude but at different radii might help to define more clearly the true character of the air motions near large thunderstorms. It would also be gratifying in future work if assumptions of the type required in estimating the flux of water vapor could be replaced with empirical data derived from improved three-dimensional observations.

ACKNOWLEDGMENTS

The author wishes to acknowledge the cooperation of the crews of ESSA's Research Flight Facility during the collection of data and the helpful discussions with NSSL staff during preparation of the manuscript. Thanks are also due to Mrs. Kathryn Gray and Mr. Tom Baxter for their help in analyzing the data and programming the numerical calculations, and to Mr. Carlos Droescher for drafting the figures.

REFERENCES

1. Baxter, T., "An Empirical Determination of the WSR-57 Radar Range Attenuation Function for Oklahoma Thunderstorms," Proceedings of the 12th Conference on Radar Meteorology, American Meteorological Society, 1966, pp. 67-70.

2. Braham, R. R., Jr., "The Water and Energy Budgets of the Thunderstorm and Their Relation to Thunderstorm Development," Journal of Meteorology, Vol. 9, No. 4, 1952, pp. 227-242.

3. Browning, K. A., "Airflow and Precipitation Trajectories Within Severe Local Storms which Travel to the Right of the Winds," Journal of the Atmospheric Sciences, Vol. 21, No. 6, 1964, pp. 634-639.

4. Byers, H. R. and R. R. Braham, Jr., The Thunderstorm, U. S. Government Printing Office, 1949, 287 pp.

5. Fujita, T., "Formation and Steering Mechanisms of Tornadic Cyclones and Associated Hook Echoes," Monthly Weather Review, Vol. 93, No. 2, 1965, pp. 67-78.

6. Fujita, T. and J. Arnold, "Preliminary Result of Analysis of the Cumulonimbus Cloud of April 21, 1961, Mesometeorology Project Research Paper #16, Department of Geophysical Sciences, University of Chicago, Feb. 1963, 16 pp.

7. Fujita, T. and H. R. Byers, "Model of a Hail Cloud as Revealed by Photogrammetric Analysis," Nubila, Vol. 5, No. 1, 1962, pp. 85-105.

8. Fujita, T. and H. Grandoso, "Split of a Thunderstorm into Anticyclonic and Cyclonic Storms and Their Motions as Determined from Numerical Model Experiments," Satellite and Mesometeorology Research Project Paper #62, Department of Geophysical Sciences, University of Chicago, Oct. 1966, 43 pp.

9. Goldman, J. L., "The Role of the Kutta-Joukowski Force in Cloud Systems with Circulation," Technical Note 48-NSSL 27, National Severe Storms Laboratory, June 1966, pp. 31-34.

10. Milne-Thomson, L. M., Theoretical Hydrodynamics, (4th Ed.) The Macmillan Co., New York, 1960, 660 pp.

11. Newton, C. W., "Dynamics of Severe Convective Storms," Meteorological Monographs, American Meteorological Society, Vol. 5, No. 27, 1963, pp. 33-58.

12. Newton, C. W., "Circulations in Large Sheared Cumulonimbus," Tellus, Vol. 18, No. 4, 1966, 14 pp.

13. Newton, C. W. and J. C. Fankhauser, "On the Movements of Convective Storms, with Emphasis on Size Discrimination in Relation to Water Budget Requirements," Journal of Applied Meteorology, Vol. 3, No. 6, 1964, pp. 651-668.

14. Newton, C. W. and H. R. Newton, "Dynamical Interactions between Large Convective Clouds and Environment with Vertical Shear," Journal of Meteorology, Vol. 16, No. 5, 1959, pp. 483-496.

15. Staff Members, NSSP, "Environmental and Thunderstorm Structures as Shown by National Severe Storms Project Observations in Spring 1960 and 1961," Monthly Weather Review, Vol. 91, No. 6, 1963, pp. 271-292.

GPO 834-818